Thermal Cycling Of LTO||LCO Batteries Subjected to Electric Vehicle Schedule and Its Second Life Evaluation

by

Harshwardhan Wadikar

A Thesis Presented in Partial Fulfillment
of the Requirements for the Degree
Master of Science

Approved May 2019 by the
Graduate Supervisory Committee:

Peter Crozier, Chair
Qing Hua Wang
Qiong Nian

ARIZONA STATE UNIVERSITY

August 2019

ABSTRACT

Lithium Titanium Oxide (LTO), is a crystalline (Spinel) anode material that has recently been considered as an alternative to carbon anodes in conventional Lithium-Ion Batteries (LIB), mainly due to the inherent safety and durability of this material. In this paper commercial LTO anode 18650 cells with Lithium Cobalt Oxide (LCO) cathodes have been cycled to simulate EV operating condition (temperature and drive profiles) in Arizona. The capacity fade of battery packs (Pack #1 and Pack#2), each consisting 6 such cells in parallel was studied. While capacity fades faster at the higher temperature (40°C), fading is significantly reduced at the lower temperature limit (0°C). Non-invasive techniques such as Electrochemical Impedance Spectroscopy (EIS) show a steady increase in the high-frequency resistance along with capacity fade indicating Loss of Active Material (LAM) and formation of co-intercalation products like Solid Electrolyte Interface (SEI). A two-stage capacity fade can be observed as previously reported and can be proved by differential voltage curves. The first stage is gradual and marks the slow degradation of the anode while the second stage is marked by a drastic capacity fade and can be attributed to the fading cathode. After an effective capacity fading of ~20%, the battery packs were disassembled, sorted and repackaged into smaller packs of 3 cells each for Second-Life testing. No major changes were seen in the crystal structure of LTO, establishing its electrochemical stability. However, the poor built of the 18650-cell appears to have resulted in failures like gradual electrolytic decomposition causing prominent swelling and failure in a few cells and LAM from the cathode along with cation dissolution. This result is important to understand how LTO batteries fail to better utilize the batteries for specific Secondary-life applications.

DEDICATION

This thesis is dedicated to my parents, Ranjana Wadikar and Abhijeet Wadikar whom I revere for their selfless attempts in making me a better human. This would not have been possible without their moral support and belief in me. I salute the unconditional love of every parent towards their child.

ACKNOWLEDGMENTS

Foremost, I would like to thank my advisor Dr. Peter Crozier. He has not only instilled a research acumen in me, but also a professional attitude that will help me henceforth in life. I am thankful to him for his constant belief, support, motivation and patience throughout my learning process. I can't thank him enough for being so accommodating and supportive throughout my academic endeavors.

I am also grateful to my committee member Dr. Qing Hua Wang and Dr. Qiong Nian for spending time to read this thesis and providing their insightful comments and for the words of encouragement which have helped in boosting my confidence. I express my sincere gratitude and acknowledgments to thank SEMTE faculties who are behind the wisdom I have acquired. I would also like to thank Dr. Terry Alford, Dr. Seffatin Tongay, Dr. Sandwip Dey, Dr. Fernando Ponce and Dr. Jim Hartman for always being there to help students in need and propagate values worth endorsing. Finally, I would like to express my gratitude towards Andrea Brown, my academic advisor for her help and counsel, and all the non-teaching staff of ASU for being the backbone of this institution.

TABLE OF CONTENTS

Page

CHAPTER Page

LIST OF TABLES

LIST OF FIGURES

NOMENCLATURE

CD	Charge Depleting
EIS	Electrochemical Impedance Spectroscopy
ESS	Energy Storage System
EV	Electric Vehicle
HWFET	Highway Fuel Economy Test
IEA	International Energy Agency
LAM	Loss of Active Material
LCO	Lithium Cobalt Oxide
LFR	Low Frequency Range
LIB	Lithium Ion Batteries
LLI	Loss of Lithium Inventory
LMCO	Lithium Manganese Cobalt Oxide
LTO	Lithium Titanium Oxide
NCM	Lithium Nickel Manganese Cobalt Oxide
RUL	Remaining Useful Life
SC-03	A type of Supplemental Federal Test Procedure (Air Conditioning)
SoC	System on Chip
SEI	Solid Electrolyte Interface
UDDS	Urban Dynamometer Driving Schedule
US-06	A type of Supplemental Federal Test Procedure

1 INTRODUCTION

1.1 History

Although the term ‘Battery’ was first used by Benjamin Franklin to describe a set of capacitors he had connected in series to produce a higher voltage, the term is now used to define a single or connected set of electrochemical cells that can convert stored chemical energy into usable electricity. The first battery is known to have existed over 2000 years ago, the Parthian battery or the Afghan Battery that used an Iron rod inside a Copper cylinder, packed inside an earthen clay pot is speculated to have been used for electroplating [1]. However, the first definitive battery is known to be built by Alexander Volta in 1800 by separating Zinc and Copper plates by cloth soaked in saltwater. Being higher in the reactivity series, Zinc oxidizes easily and thus acts as anode as compared to copper which acts cathode in the electrochemical cell. Like many natural phenomena like photosynthesis and respiration, batteries work on a redox reaction. In 1802 William Cruickshank modified the ‘Voltaic pile’ for mass production of the ‘Trough’ battery that laid the voltaic pile to its side in a slotted box to avoid electrolyte leakages.

In 1836, John Fredric Daniell further improved the design of batteries by using a porous earthen pot barrier separating Copper cathode immersed in copper sulphate kept inside Zinc anode container with Zinc sulphate. The porous barriers improved ion mobility and prevented hydrogen bubbles that improved the operation times and reliability [2]. In fact, the unit of 1 Volt is derived from the output of a Daniel cell [3]. It was in 1859, when French physicist Gaston Planté fabricated the first secondary(rechargeable) battery, using Lead (Pb) anode and Lead Oxide cathode (PbO_2) submerged in sulphuric acid. Despite being very heavy and environmentally toxic, these batteries are used in cars today due to the robustness of this model against high rate capabilities [4].The first

dry battery was invented by Carl Gassner, consisted of a carbon cathode and a Zinc anode separated by a dry electrolyte paste of aluminum chloride and plaster of Paris.[5] Since it could be used in any orientation, owing to its dry nature, it got widespread attention and was commercialized and the design has continuously improved leading to the modern alkaline battery[6]. Even today the design and materials used widely vary, the working of battery has still relied upon the same fundamental chemistry of redox reactions.

1.2 Relevant Background

Important breakthroughs in the past century by prominent scholars like British chemist M Stanley Whittingham [7] John B Goodenough [8], also known as the father of Li-Ion Batteries (LIBs), have yielded energy storing crystalline materials that has ushered humanity towards a brighter future. This led to the commercialization of primary (single use) LIBs in 1991[9] and further the commercialization of Lithium Polymer (Li-Po) batteries [10]. Global concerns like climate change has led to electrification of technology and batteries are becoming common commodity. In this decade itself, the costs of batteries have reduced from $1000/KWh in 2010 to $275/KWh in 2016[11]. This is driven by the everchanging landscape of energy storage; however, Lithium remains as the active charge carrier alternative due to low weight density and high electrical potential. Figure 1 shows a schematic of a standard LIB, consisting of carbon anodes and Lithium Cobalt Oxide cathodes, packed in a cylindrical format. Cylindrical cell formats are a popular choice of

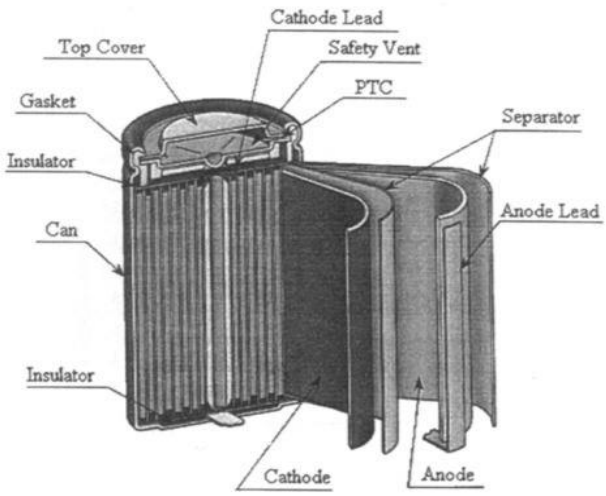

Figure 1: Schematic of a Lithium Ion Battery [12]

automakers for making larger battery modules as this format ensures ample surface area for Li^+ shuttling and better manufacturability. The kind of materials used as electrodes determine the nominal voltage while the amount of active materials defines the gravimetric and volumetric energy densities of the cell.

The main concern of using conventional cells that use a carbon anode in a vehicle is the associated with lithium plating and dendrite formation at the anode, recent efforts to address this issue include printing LTO slurries on Solid State Electrolytes like Lithium Lanthanum Zirconium Oxide [13]. As the chemistry and format are crucial to the performance of LIBs, it is important to characterize and study different formats (Cylindrical, Pouch, Coin, Prismatic) and newer materials.

A Ragone plot describes the power packed in a cell with its weight with a volume it takes for storage, figure 2 shows a plot of volumetric energy density Vs gravimetric energy densities of relevant Li-Ion LTO chemistries.

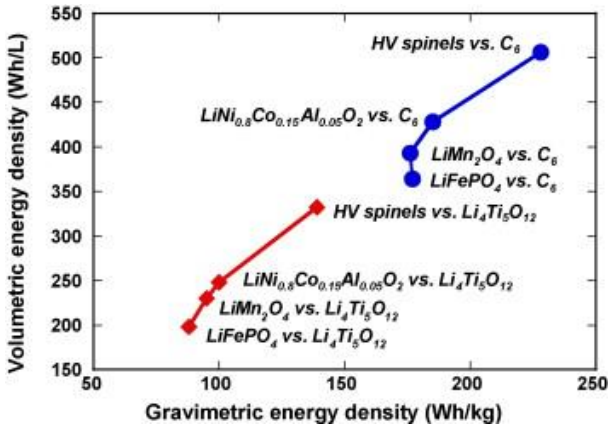

Figure 2: Energy per unit volume of various chemistries [14]

Note that the values in this plot considers the overall weight of cells and not just the active materials. Although the Gravimetric energy density for LTO anodes is lesser than that of conventional carbon anodes, LTO anodes have many desirable battery characteristics like safe

discharge even at high current rates and better structural stability. Carbon has been the choice of EV manufacturers (Tesla, Nissan) while the cathode material has been improved from LCO to LMNO to LFP (Olivine structure). For a given chemistry and format, battery operation is affected by ageing and is subordinate to the operating conditions like the current-rate and working temperature. With growing number of chemistries being developed together the testing of any commercial cells should thus consider the intricacies of redox reactions. Half cells of active materials should be studied under controlled environment before being mass produced. However, this is out of the scope of this document This study was constrained by the SRP project that required testing battery packs further development is dedicated to electronics required for charging and a designing load circuit that can test single cells. The way a cell reacts electrochemically is dependent on the way it is used (i.e. charging pattern, temperature), it should be calibrated and parameters should be measured when the cell is being relaxed from the load.

1.3 Literature Survey

Climate change and rising levels of greenhouse emissions from conventional vehicles have led the automotive industries to move towards electrification of vehicles that have Energy Storage Systems (ESS) made up of Li-Ion Batteries (LIBs). A sustainable utilization of these ESS is a major concern as they are extensively being used in consumer electronics, grid energy and storage and now, transportation [15]. International Energy Agency (IEA) estimates that the number of Electric Vehicles (EVs) to rise from 3.7 million currently to 21.5 million EVs by 2030 [16]. With the growing demand of such vehicles, developing cost-effective and long-lasting batteries that are safe is crucial to the sustainability of this benevolent transition. Since the commercialization of LIBs in 1991 by Sony® that used $LiCoO_2$ cathodes and graphitic anodes, many new cathode materials like $LiMn_2O_4$ (spinel) $LiFePO_4$ (olivine), $Li_{1+z}(Ni_xMn_xCo_{1-2x-y}Ti_y)\ O_2$, however, very few changes have been made in the anode side of the cell, in terms of material innovation or chemistry [17-18]. The current state of LIBs, that are used in electric vehicles still uses a carbon anode and a stabilized blend of lithium- transition metal oxide and they still fall short to deliver a safe, long-lasting power backup. With growing concerns of safety and cycle-life, an alternative to inflammable lithiated graphite (charged) is crucial is to study and establish to supplement the rapid electrification of vehicles. Considering that battery modules currently contribute 40% of an electric car's worth, it also becomes important to actively diagnose the State Of Health (SOH) of the ESS and model its capacity fade mechanism for second-life applications of ESS from Gridable Vehicles (GV)[19]. As the performance of the battery is primarily dependent upon the format and chemistry used, individual cells as well as larger packs from such Gridable Vehicles should be studied to better estimate the Remaining Useful Life (RUL).

Lithium Titanium Oxide (LTO spinel), a novel garnet-based anode material has recently gained much attention due to its excellent structural stability, self-passivating thin layered SEI formation [20], zero strain property, long cycle life and better safety features [21]. $Li_4Ti_5O_{12}$ (stoichiometrically, $Li[Ti_{1.67}Li_{0.33}]O_4$) has a stable spinel structure with crystallographic sites denoted as $[Li_3]^{8a}$ [$Li_1Ti_5]^{16d}$ $[O_{12}]^{32e}$ and has space group of Fd-3m which can take up to 3 Li+ per molecule and change to $Li_7Ti_5O_{12}$ as per the following reaction with a theoretical capacity of 175 mAh/g [22-23].

$$Li_{3(8a)}\,[LiTi_5^{4+}]_{(16d)}\,O_{12(32e)} + 3e^- + 3Li^+ \leftrightarrow Li_{6(16c)}\,[LiTi_3^{3+}Ti_2^{4+}]_{(16d)}\,O_{12(32e)}$$

During this reaction, the tetrahedral(8a) Li^+ ions are displaced into neighboring octahedral(16c) sites to generate a rock salt structure with all the octahedral sites are occupied by the) Li^+. During this lithiation(charging) process, the spinel framework remains intact. The interstitial space of the spinel framework provides a three-dimensional network of the 8a tetrahedra and 16c octahedra through which lithium ions can diffuse rather unrestricted through the interstitial space, thus allowing rapid lithium-ion transport. Ab-initio calculations suggest that $Li_4Ti_5O_{12}$ can bear a theoretical capacity of 262 mAh/g transforming into $Li_{8.5}Ti_5O_{12}$ when charged from 0 to 3 V by insertion of extra lithium in the empty 8a sites which is accompanied by a negligible 0.4% volume change [24]. However, our study limits the battery charging to 2.75 V and thus this phase change is out of the scope of operation although it might occur in cases of overcharging. Figure 3 shows the Schematic of the spinel structure with atoms shown in the upper half depict the positions of lithium and titanium cations at 8a(Stripped spheres) and 16 d (dark dots) surrounded by the Oxygen anions as clear circles occupying 32e position in the lattice of LTO.

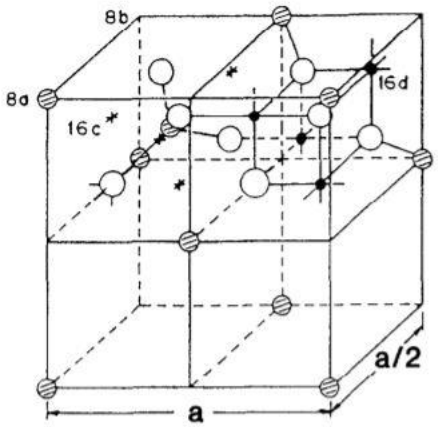

Figure 3: Schematic of LTO Spinel structure [25]

It is noteworthy that Li-poor $Li_4Ti_5O_{12}$ has a spinel crystal structure with very low electronic conductivity while Li-rich $Li_7Ti_5O_{12}$ has a rock-salt crystal structure and has comparatively higher electronic conductivity. This differential in conductivities prevent an internal short circuit and a gradual cause thermal runaway and thus are inherently safe [26].When Li ions are extracted from Li-rich rock-salt phase, it gets consumed of Li ions rapidly, being highly conductive phase and transforms into spinel phase, which increases the impedance preventing a spike of Li ion starvation as caused in carbonaceous anodes at high C rates. However, the electrochemical properties of LTO, like carbon, greatly depend on the hierarchy of the structure and requires tuning of nanoparticles and mesoporous aggregates to stay at its maximum capacity. LTO is a material of interest to many scholars not only because it can be used in next generation Solid State Batteries that use flexible inflammable ion-conducting separator membranes (Gel Composite Electrolytes) and using multi-stage printing with LCO cathodes [27] but also because composites like LTO-TiO_2 can efficiently shuttle Na+ ions in Sodium Ion Batteries (SIBs) against a sodium metal [28]. LTO batteries are already used in Honda, Mitsubishi [29] and are been used in projects like TOSA [30] and are available in various formats like prismatic, pouch, cylindrical 18650s [31].

However, the basic working of LTO batteries is same and can be visualized using the next

following Figure 4.The octahedrons in LTO are formed by Oxygen atoms at the edges around a Titanium cation , lithium ions are shown by dark spheres. The Li ions thermodynamically prefer to reside and orient inside the bulk of the positive electrode(cathode) which is usually a Lithium-Transition metal oxide layered structure, where Lithium ions can reside between layers . During charging, the Li ions are forced into the anode (LTO in this case) and remain in a dynamic equilibrium which is controlled by the external electron flow.

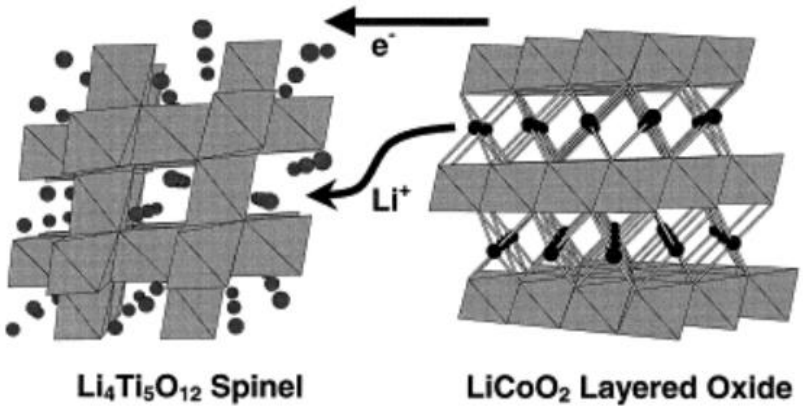

Figure 4: Working of LTO||LCO cell [26]

With the external circuit turned on, the flow of electrons is the cause of Li ions shuttling back from anode to cathode through the electrolyte.

With growing EVs on road, the determination of the State Of Health (SOH) of a battery pack/ESS by on-board diagnosis that can be estimated using Battery Management System (BMS) has become crucial [32]. Since ageing of Li-ion batteries in EVs being dependent upon driving patterns, discharge rate, temperature and battery chemistry this study focusses on LTO||LCO which are subjected to custom duty cycles that mimic typical drive conditions for an EVs to evaluate its true performance and failure modes using invasive and noninvasive techniques and explore the need of an active thermal management of the ESS. After a capacity fade of 20%, battery packs were dissembled and repackaged into smaller packs and were cycled under step wave form cyclic

thermal load to simulate seasonal changes, to explore the viability of LTO batteries in Second-Life applications. This approach emphasizes on reusing faded batteries before their End-Of-Life with a range of applications from smart grids that reuse ESS for auxiliary storage for solar systems [33]. Overcharge durability during cycling and ageing at room temperature, for LTO batteries has been studies previously [34-35].

1.4 Scope and Objective

Battery manufacturers provide a data sheet with cell performance, often under Constant Current Constant Voltage (CC-CV) conditions. The procedure includes charging and discharging at a constant current between fixed voltage limits. This does not represent the dynamic nature of load as experienced by battery module in an electric vehicle. Real-time cycling under simulated loads and environment is the key to get conclusive results about battery life. Battery characterization is an emerging field that has just recently gained much attention, as batteries of diverse chemistries and formats are widely manufactured. While the proponents of testing batteries with DC load like Prof. Jeff Dahn(with Tesla and Panasonic) use high precision direct current sources to find coulombic efficiencies as the cells are cycled in real-time to attribute the capacity fade to unwanted interface formation, other scholars like Prof Han (Tsinghua University, China) utilizes Differential Voltage curves to probe State Of Health in a manner that is convent for on-board continuous monitoring . [36-37]. Modern testing of batteries includes extended characterization that run different schedules on cycler that run different kinds of tests for values of Static Capacity tests, SoC, OCV using active filters. [38]. Most of these approaches can be implemented on-board with the ESS so that continuous monitoring is possible, unlike EIS that requires testing when operation is ceased. The premise of the study lies on the fact that batteries

should undergo real-time tests before being considered for any application, thus a parallel assembly of 6 cells in parallel was used for testing. The objective of this study is to simulate real-time conditions and implement battery characterization techniques such as Capacity Fade, Differential Voltage, EIS and XRD to determine the failure mechanism in LTO anode LIBs . As LTO batteries are been used in Electric Vehicles it is essential to understand if we can apply the conventional model of carbon-anode battery degradation to estimate Remaining Useful Life (RUL). The manufacturer of the cells is kept confidential since no permission to cut cells for study was acquired.

The following equation has widely been used to model batteries that have carbon anodes, where , Q_{loss} is the percentage capacity loss; E_a is the activation energy in J/mol; R is the gas constant; T is temperature in kelvins; t is the cycling time; z is the power law factor; and B is the pre-exponential factor. However, such a model might not hold true to yield a correct RUL when the

$$Q_{\text{loss}} = B \exp\left(\frac{-E_{\text{a}}}{\text{R}T}\right) t^{z}$$

cell under consideration has a different chemistry [36]. It is thus important to model specific battery chemistries to practically predict RUL. With these objectives this study aims to find the feasibility of using LTO batteries in EVs

An approximate mechanism of capacity fading will provide the basis of application and feasibilty in second life. In a sustainable energy scenario, large ESS would be actively monitored and reused after they are unable to deliver acceptable capacity. This would not only promote safety but also the life cycle of the commodity.

On testing of batteries that are thermally cycled after a few hundred cycles (as in this study) to simulate prolonged seasonal effects along with drive schedules that require high instantaneous discharge charge rates, causing an accelerated aging. A capacity fade mechanism that is unique to LTO anodes and distinctively different from failure in carbon anode batteries is confirmed. Effects of temperature on cell performance and need for thermal management is also investigated for LTO cells,

2 EXPERIMENT

2.1 EV Drive Protocols

In this study, LTO anode commercial batteries are tested under a custom drive cycle (AZ01), for state of Arizona, that combines several standard drive protocols like UDDS (urban driving), HWFET (highway driving), US-06 (aggressive driving) and SC-03 (driving with air-conditioning). The velocity profile of this cumulative cycle is shown in Figure 5 with an average velocity of 21.74 miles per hour, covering 16.4 miles.

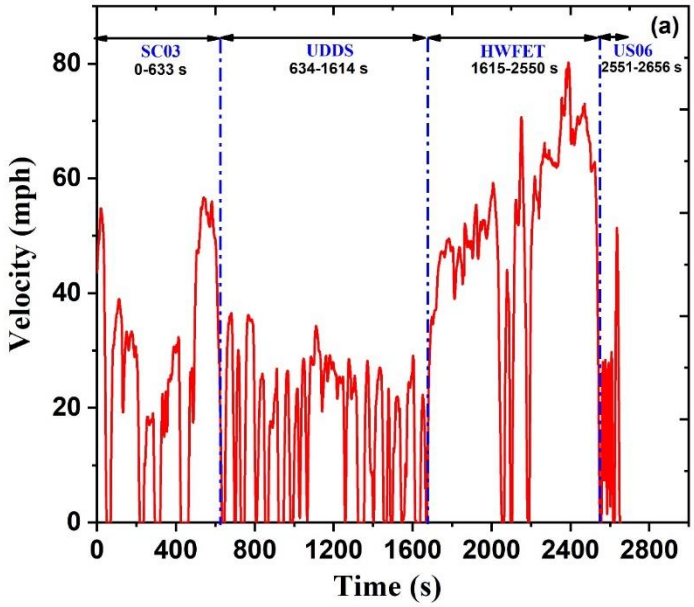

Figure 5: Composite Driving profile, AZ-01

Since the battery pack will be the sole power source for an EV, a Charge-Depleting (CD mode is selected for cycling the packs with a Depth of Discharge of 80%. The current profile for AZ-01 under the CD mode is shown in Figure 6. Furthermore, the regenerative breaking was limited to 7% in the current profile to get the battery packs discharges faster. Appendix A shows simulated current profile for a 300 mile ranged, mid-sized all electric car in Argonne National Lab's Autonomie.

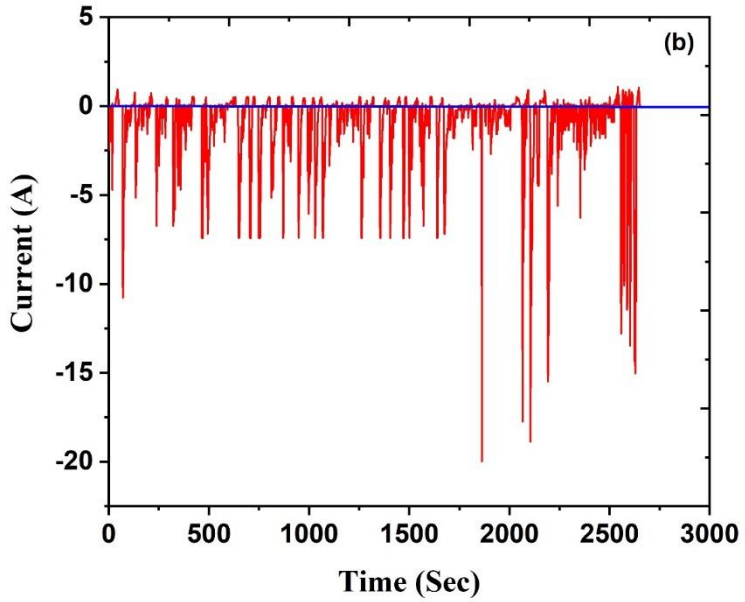

Figure 6: Current Profile for AZ-01

A detailed procedure to derive current profiles was retrieved, studied, and published by Peterson *et al* [39]. The current profile was scaled to fit +/- 20 ampere current range for an Arbin cycler (BT2000) shown in Figure 7 and was used to record data points for capacity fading.

As per the manufacturer, each cell has the positive electrode as Lithium Cobalt Oxide (LCO) while the negative electrode is made up of Lithium Titanium Oxide (LTO). Each cell is rated capacity of 1300 mAh and operate at a nominal voltage of 2.4 V, with a cutoff voltage of 2.85 V.

Figure 7: Arbin BT-2000 Cycler

Two battery packs (Pack # 1 and Pack # 2), each containing six of such cells connected in parallel with cumulative capacity of 7.8 Ah were used to make battery packs to be subjected AZ-01 cycling in temperature chambers. Initial values of capacity of battery pack were determined by discharging the packs at C/2 (3.9 A) between fixed upper (2.85 V) and lower (1.5 V) voltage, for 5 cycles with 5 min rest in between using Arbin BT 2000 cycler charge and discharge at room temperature.

2.2 Battery cycle-life test and second life

Both battery packs were cycled at 40°C and 0°C temperatures to see the effect of temperature on the performance and life these LIBs. To replicate the seasonal changes in temperatures, each pack was cycled for a few 100 cycles before switching the temperature. Figure 8 shows the flowchart for the schedule in Arbin cycler. Battery pack is first charged up to 2.85 V at a 1C rate following a rest of 5 minutes after which the battery is discharged using the AZ-01 current profile.

This process is carried out 6 times before charging and discharging the battery at C/5 rate with 10 minutes rest. The Arbin is programmed to carry out this in loop of 6. In final step, battery pack is again charged up to upper cut off voltage at 1C rate. Typically, one such schedule takes ~ 37 cycles and it takes about a week or more to complete the schedule depending upon the operational temperature.

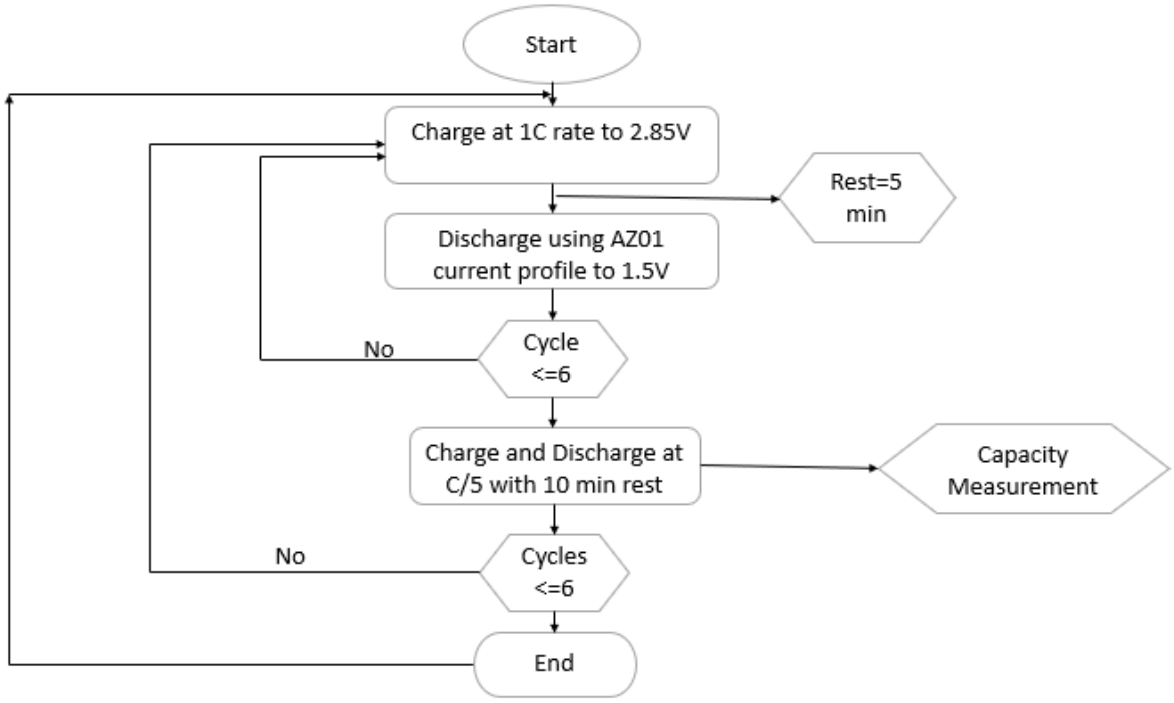

Figure 8: Flowchart for the cycling schedule

Reusing batteries, that are no longer adequate for use in EV, can have a major impact on environment and battery recycling industry Apart of developing techniques for recycling LIB, there is also a need to reuse these batteries for second life applications. These applications can be energy storage for residential usage, micro-grids or auxiliary ESS for load shaving [40]. After AZ01 cycling, half of battery packs were subjected to second life testing. Batteries were cycled under constant current charge/discharge current C/2 rate. For this, “8 channel battery analyzer”, shown in Figure 9 from ‘Battery Space’ was used, that could provide 3A of current up to 5V on

each channel. Both battery packs were cycled at C/2 current rate at 0ºC and 45ºC.

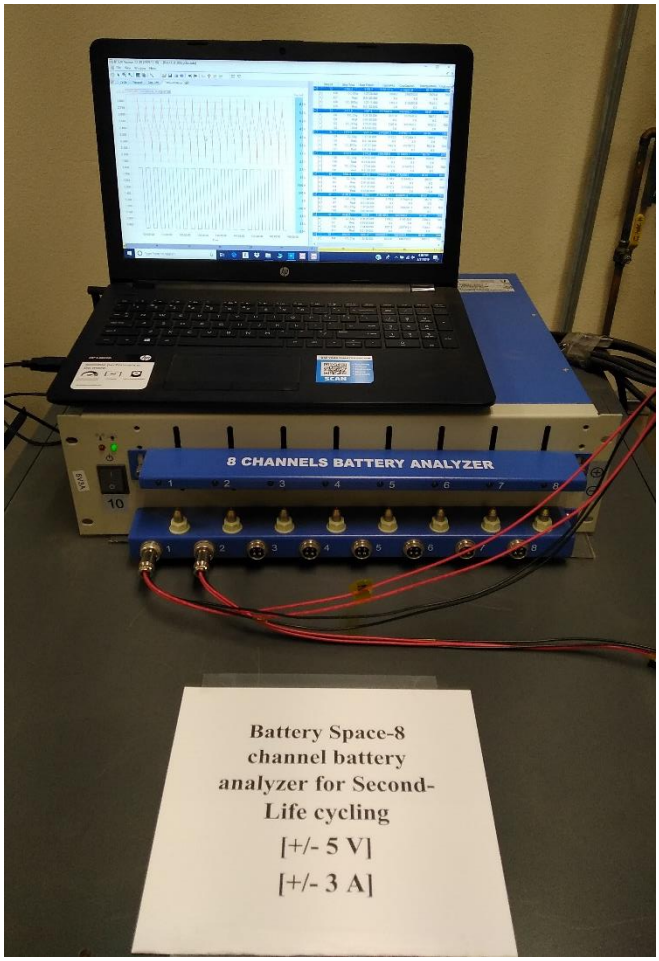

Figure 9: Battery Space 8-Channel Battery Analyzer

3 CHARACTERIZATION

3.1 EIS Analysis:

Electrochemical Impedance Spectroscopy (EIS) measures the impedance of a system over a range of voltage perturbation at various frequencies, and the frequency response reveals the properties of the system. This is one of the most widely used non-invasive technique to quantitively estimate the temperature gradients and relaxation [41] and State Of Charge (SOC) [42] of LIBs based on frequency response of signal. The EIS patterns were fitted using the circuits seen in the inset of following figures. The Nyquist plot of battery consists of three distinct regions, each representing a part of the Rendall's circuit. Firstly, an inductive tail to the left of a Nyquist plot at high frequency that intercepts with Z_{re} axis denotes High Frequency Resistance (HFR) representing ohmic resistance in series with the cells offered by the battery pack and the total pack inductance. This includes summation of all resistances offered by electrolyte, current collectors, electrode particles and connections between cell terminals and instrument. Second feature is marked by a semicircular region at mid frequency range that is attributed to charge transfer resistance of Li^+ through the Anode-Electrolyte Interface (a.k.a. SEI) and Cathode Electrolyte Interface (CEI). Third region includes a tangential line, representing the impedance due to diffusion process into electrodes at lower frequency and is represented by a Warburg element in the Rendall's circuit. In this study EIS tests were carried out on cell at regular intervals of cycling. Batteries were charged up to 100% SOC after two hours being out from temperature chambers to Voltage signal of amplitude 10mV was applied over frequency range of 10KHz to 10mHz. The apparatus used for EIS test was Biologic BCS 810, shown in Figure 10. Finally, a Warburg resistance is included to account for diffusion in the Low Frequency Range (LFR).

Figure 10: Biologic 810 Potentiostat

3.2 XRD Analysis

X-Ray diffraction is an established method in Solid State characterization, that uses the order of atoms in planes (for any crystal structure) and gives the interplanar distance between planes in different miller directions. This becomes the direct link to its crystal structure and lattice parameters which also yields site occupancy. To confirm the structural integrity of crystalline electrodes, Bruker D-8 X-Ray (Copper K_α; λ=1.5406 Å) diffraction machine, shown in Figure 11, was used to probe the active material.

Figure 11: Bruker D-8 X-Ray Diffractometer

After an eventual capacity fade (~20%), the packs were sorted and repackaged into smaller packs for Secondary-Life and the rest cells were used for the invasive testing. The cells cycled on AZ-01 were discharged completely before cutting inside a fume hood. Preparing the samples includes extracting jelly roll from the metal casing after which circular blanks were cut from the electrode films. These electrolyte blanks were sonicated for 30 mins in Propylene Carbonate to remove the electrolyte salts, prior to rinsing isopropyl alcohol. After overnight vacuum drying at 80°C was done after washing. SEI cannot be probed using this approach since it too washes away during sonication. A scan from 10 to 60 degrees was carried out at a scan rate of 2 degrees per minute for structural analysis.

4 RESULTS AND DISCUSSIONS

4.1 Capacity Fading

As the two battery packs undergo thermal cycling (0 °C and 40°C) while being discharged via AZ-01, a capacity fade is observed in both the packs, depicted in Figure 12 and Figure 13. It is noteworthy that the discharge capacity drastically falls at lower temperature than at a higher temperature while the cells retain this capacity fades less with cycles at the lower temperature limit. Although cells cycled at higher temperature delivered significantly more discharge capacity, the capacity fade at this temperature is observed to be faster. A two-stage capacity fade, as previously reported for LTO batteries can be seen evidently; the first stage is marked by slow capacity fade before the onset of second stage which is marked by significant and drastic capacity fade. Pack#1 remains in the stage 1 of capacity fading under the EV schedule and shows excellent cyclability, with the maximum capacity fade at the high temperature limit~3.75% in 138 cycles. We can also say that about 290 mAh is lost from 7800 mAh over 138 cycles (or 2mAh fade per AZ-01 schedule).The capacity fade is minimized at the low temperature with about 1.1% over the next 258 cycles and it can similarly be concluded that about 61 mAh of capacity is lost from 6100 mAh available at zero degree Celsius or 0.23 mAh of capacity is faded after each cycle of AZ-01 at the lower temperature limit.

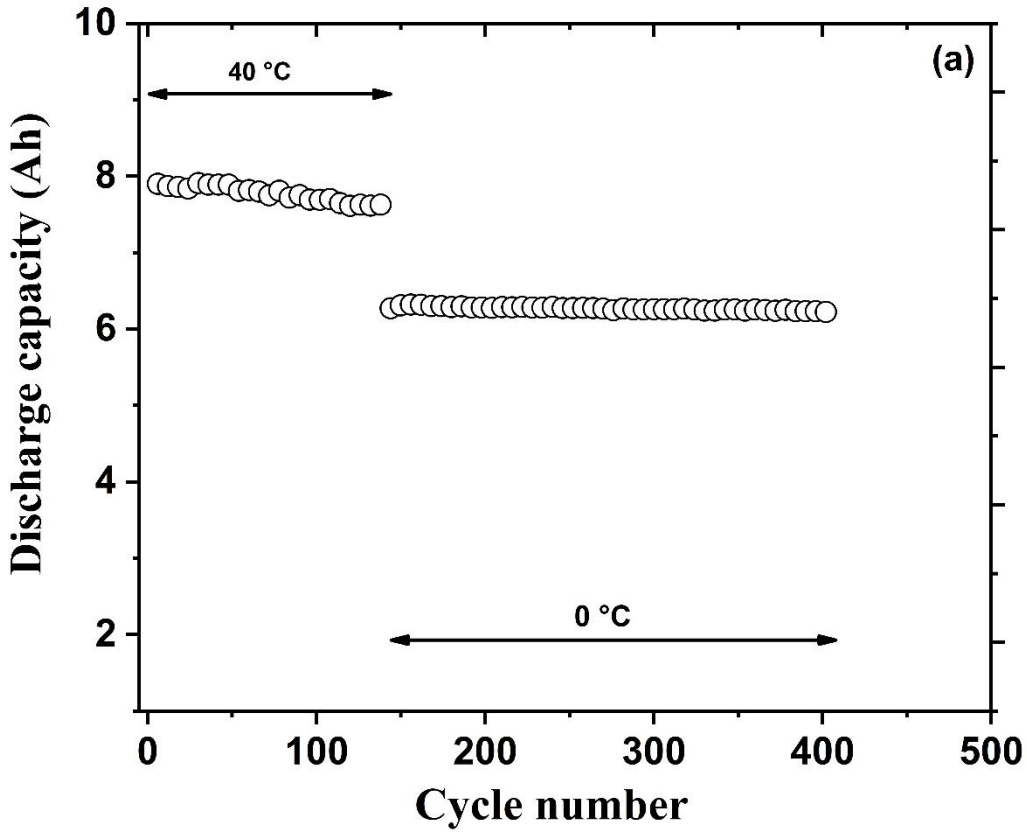

Figure 12: Capacity Fade for Pack#1 under EV cycling

Pack#2 showed the similar capacity fade of 128 mAh lost off 6400 mAh available over 174 cycles (0.73 mAh/ cycle) with overall ~2.4% fade at low temperature operation after which. major fading~6.8% over 186 cycles is observed when cycled at high temperature and it seems to enter the second stage of more drastic fading, which translates to 510 mAh lost off 7500 mAh or 2.74 mAh/ cycle. This is four times the degradation at lower temperature and can at least one cell must have reached the inflexion point of stage 1 degradation, entering into a regime of more drastic

capacity fade as evident

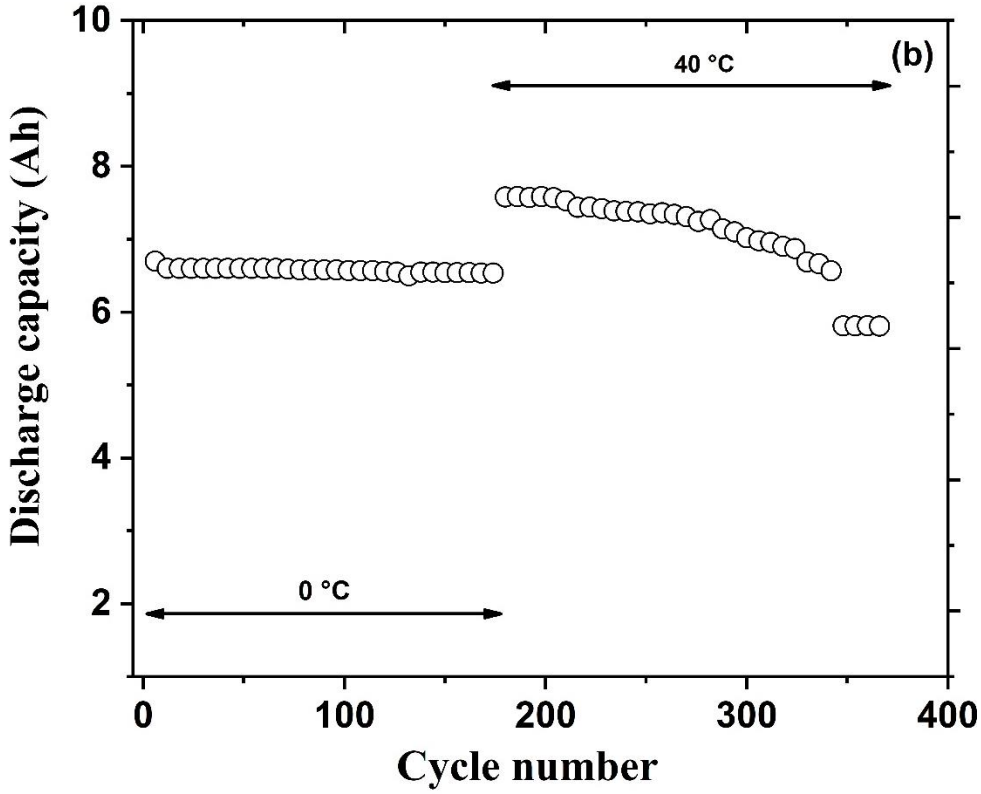

Figure 13: Capacity Fade for Pack#2 under EV cycling

After an overall capacity fade of ~20% the battery packs were disassembled, and the cells were tested. All the cells from pack#1 seemed acceptable while one cell from pack#2 was swollen up and showed a voltage output in the range of Millivolts. A picture of the swollen cell can be seen in Appendix A. Figure 14 shows capacity values for second life. Batteries were initially charged C/2 rate up to cut off voltage and discharged at C/2 rate after rest of 2 minutes.

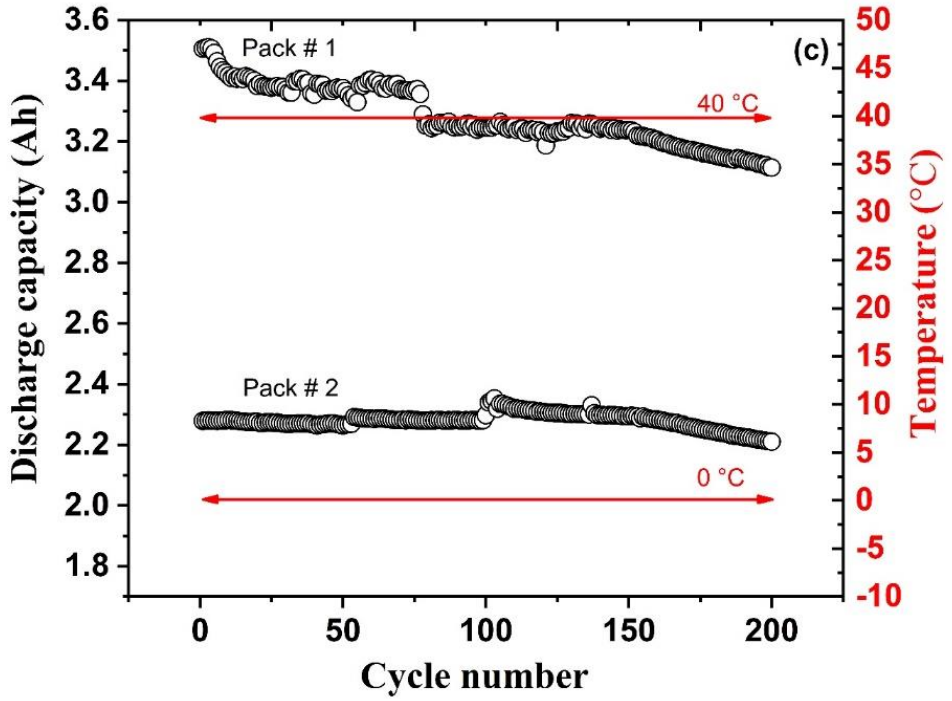

Figure 14: Capacity Fade of Pack#1 and Pack#2 for Second-Life under CC-CD at C/2 rate

4.2 Electrochemical Impedance Spectroscopy

The distinct shape of EIS spectra show a clear ionic diffusion through different part of the battery. When a cell discharges, the circuit current is the result of Li ions travelling from anode to cathode. This involves de-intercalation of Li ions from LTO (fast) followed by charge transfer from the electrolyte (most mobile ions) after which Li ions diffuse through interface (CEI) and eventually de-solvation of Li ions into the cathode. The simulated curves using equivalent circuit analysis are plotted as a function of cycle number in Figure 15 and Figure 16. The EIS spectra was analyzed using the software BT-Lab and the equivalent circuit was developed and fitted using (Randomize + Simplex) to converge at χ^2 ~0.97 after stopping at 5000 iterations. A steady increase in High Frequency Resistance (HFR), (R_1) denotes Conductivity Loss (CL) from electrolyte

degradation triggered by loss of active material from the cathode primarily by dissolution and co-intercalation with electrolyte species, that eventually get deposited over anode. No depositions were probed using microscopy on the electrode films. The model used is widely accepted and known as Adapted Randall's Circuit(ARC), however this model could not yield a satisfactory fit with the experimental data, thus quantitative conclusions from these The Nyquist plot of battery packs suggest gradual increase in series resistance (intercept with zero on real axis). The resistances of electrode-electrolyte interfaces (R_2) and charge transfer resistance(R_3) could not be resolved into two distinct semi-circles, this suggests that the battery pack should either be probed at different set of frequency of voltage perturbations or individual cells should be probed, rather than the whole battery pack with connections [43]. Table 1 and 2 show the parameters found from the EIS fit of experimental data using the model circuit as $L_1+R_1+C_2/R_2+Q_3/R_3+W_1$, also shown in the inset of plots as components of adapted Randall's circuit.

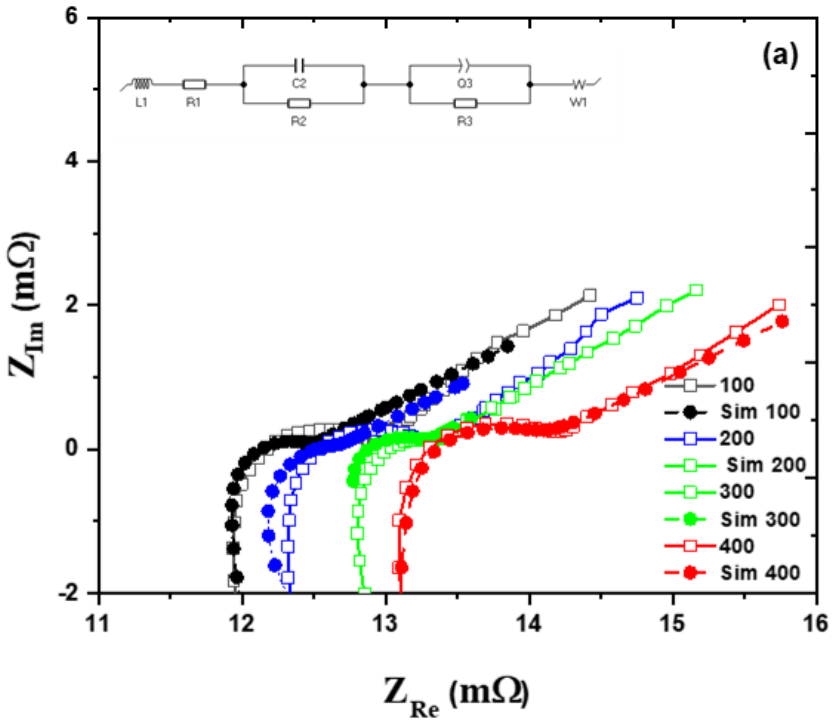

Figure 15: EIS patterns for Pack#1 under EV cycling

Table 1: Simulation parameters for Pack#1

Parameters	L_1 (H)	R_1(Ohm)	C_2 (F)	R_2(Ohm)	Q3(F.s^(a - 1))	a	R_3(Ohm)	W_1(Ohm.s-^1/2)
100	0.297 8e-6	0.01228	2.082	0.589 6e-3	-0.107	0.395 7e-6	-3.081e-3	0.552 4e-3
200	65.62e-9	0.013413	0.934	0.6956e-3	-2.708e-3	0.993	-0.0112	0.811e-3
300	28.09e-9	1.479e-2	1.914	0.768 5e-3	-0.078 36	0.690	6.905e-3	1.092e-3
400	0.314e-6	1.418e-2	0.203 8e-3	7.421e-3	6.303	0.807 9	0.948 7e-3	1.196e-3

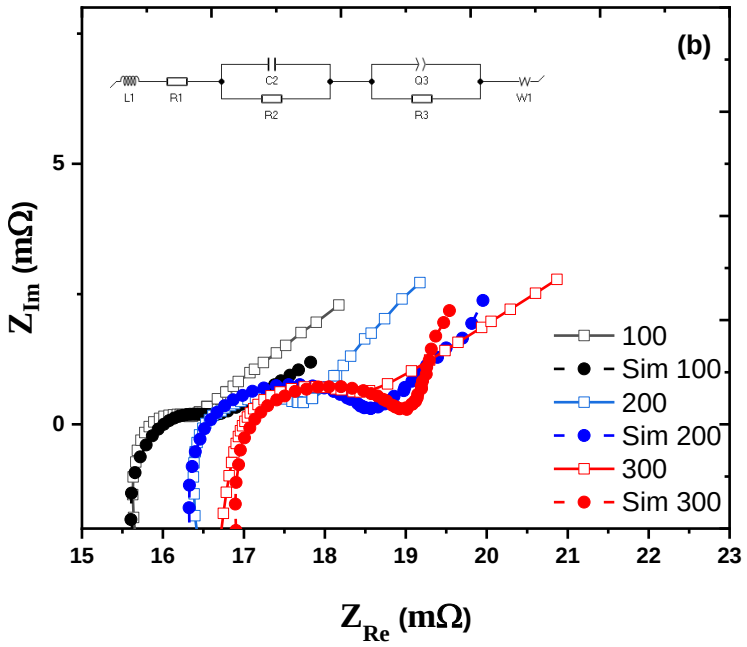

Figure 15: EIS patterns for Pack#1 under EV cycling

Table 2: Simulation parameters for Pack#2

Parameters	L_1 (H)	R_1(Ohm)	C_2 (F)	R_2(Ohm)	Q3(F.s^(a - 1))	a	R_3(Ohm)	W_1(Ohm.s-^1/2)
100	0.335 3e-6	0.01545	10.4	1.037e-3	0.070 8	0.457	0.010	1.743e-3
200	-14.73e-9	0.01647	-0.815 3e-3	-0.024	0.155	0.472	0.014	0.515 8e-3
300	0.343	0.035	4.843	0.854 2e-3	-2.844	0	-0.020 06	0.318 6e-3

4.3 Differential Voltage Curves

If a battery is analogous to a water tank with different cross-sections(capacity) at different heights (Potential). The quantity dV/dQ increases drastically(peaks) when there is a phase change of crystallite electrode bulk while a plateau is caused by steady diffusion. Although capacity fade mechanism is specific to the chemistry of a single cell, probing the electrochemical degradation of

individual electrodes can be done qualitatively by fabricating Half cells, which was beyond the scope of this study. Differential Voltage (DV) curves give an idea of the working of battery in operation and is used as an estimate of State of Health (SOH) in this regard. The peaks of DV curves represent stable phases A two phases change as previously reported for LTO battery is observed, denoted by the two peaks corresponding to Spinel and Rock-Salt structure.

For instance, since at the beginning of the battery life, cathode capacity is higher that the anode capacity, the cell capacity is limited by the anode. The first stage of gradual capacity fade is marked by the slow degradation of cathode, this stage is marked by Loss of Lithium Inventory (LLI) and Loss of Active Material (LAM)primarily and shows itself in the right side of the DV curves. As the cell ages, cathode fades faster and when its value reduces than that of anode, a second stage of capacity fade is observed which corresponds to the dwindling cathode capacity. The second stage is hypothesized to be due to failure of cell because of electrolytic reduction at the anode and formation of interfacial surfaces resulting from both LLI and LAM [44]. Similar DVA curves have been found particularly true for LTO batteries. Figure 17 and Figure 18 illustrates the DV curves observed from Pack#1 and Pack#2 discharge cycles as they get aged over the AZ-01 drive schedule with a voltage width of 10 mV, the graph is smoothened to filter noise. The degradation of the cells can be seen evidently from the capacity loss in the DVA curves.

By measuring the IC curves (dQ/dV) and differential voltage (DV) curves (dV/ dQ) estimates of State Of Health (SOH) can be predicted and are viable option for on-board Battery Management Systems (BMS) [45].

Hall et *al* [46] carried out studies on LTO||NCA batteries for stationary energy storage applications subjected to thermal cycling and varying C rates. While the LTO was stable with cycling, NCA was found out to be dominant ageing component with formation of nickel oxide

layer.

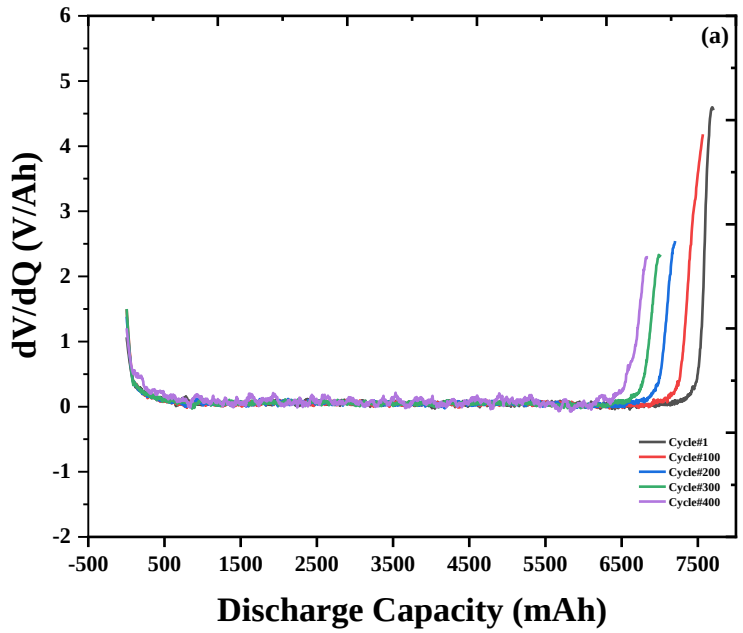

Figure 17: Differential Voltage curve of Pack#1 for EV cycling

Xuebing Han *et al* [36-37] has widely been studied to model capacity fade mechanisms similarly for various commercial LIB chemistries like LTO||NMC and C||LFP batteries using this approach. Battery ageing is attributed to two causes; Loss of Active Material (LAM) and Loss of Lithium Inventory (LLI). The former is caused by dissolution of electrode ions.

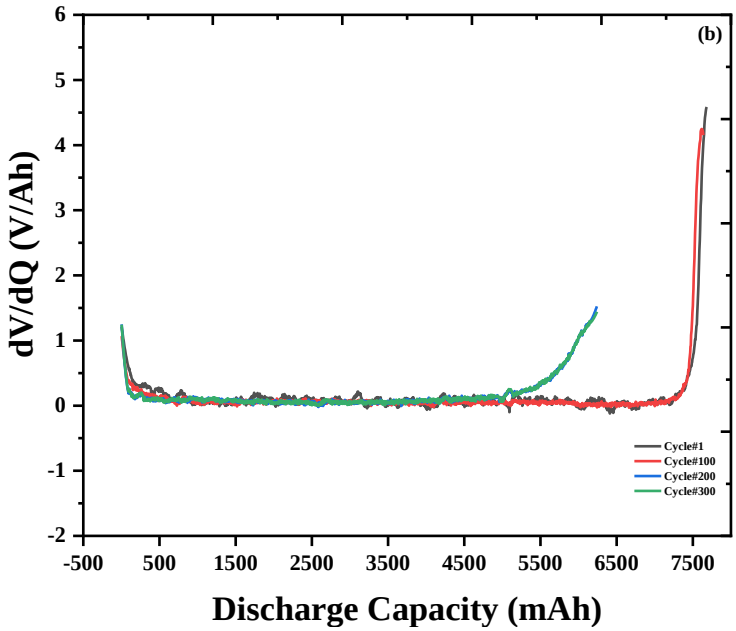

Figure 18: Differential Voltage curve of Pack#2 for EV cycling

in the electrolyte and eventual thickening of Cathode-Electrolyte Interface layer while the latter is marked by Lithium plating and SEI formation (loss of lithiated cathode). However, LLI is significantly mitigated since LTO avoids lithium plating as compared carbon-anodes and is known to have stable-thinner SEIs. Initially the battery capacity is limited by the anode capacity as the cathode that has a higher capacity but fades at a faster rate than the anode, eventually coming to a point where cathode capacity becomes less than anode capacity and is then cell capacity gets limited by the cathode capacity. The shifting of peaks on the right towards left with ageing can thus be attributed to LAM. Different LTO batteries were tested to collect Incremental Capacity (IC) and Differential Voltage (DV) data to confirm a two stage piecewise linear capacity loss which is different from traditional graphite anode degradation. Region B and C are most affected by ageing, While region. The capacity fade as observed by this research group for LTO anode cells is depicted in Appendix B.

4.4 X-Ray Diffraction Pattern

The signals from Bruker D-8 (Cu K_α source) were used to do Rietveld analysis using Topaz V4.2 with a Pseudo Voigt Function and an LP factor with a monochromator angle of 26.4°. Chebychev polynomial of 5th order with 1/X Bkg function was used to filter the background. The reference used of LTO [47] and LCO [48] is obtained from Open Crystallography Database. The patterns for Anode and Cathode can be seen in Figure 19 and Figure 20. The structural analysis and phase detections were done using the Jade software. The XRD patterns of LTO shows no major change in the crystal structure. The Rietveld refinement reveals minor changes in the lattice constants and negligible strains as expected are confirmed. The swollen cell from pack#2 exposed the delaminated anode film and a 5% loss of weight was observed, which is an indication of failure by gassing. Although no other cell showed major swelling and similar fading. However, the XRD of the cathode reveals that the cathode material is a mix of LCO and LMNCO.LCO is known to be tuned and mixed with LMNCO to electrochemically outperform LCO, when the ratio of LCO and LMNCO is about 80:20[49] As the battery is cycled the loss of Mn ions is seen, which is commonly observed[50] and shows that the Li ion transport occurs through a solid solution method rather than through phase change as seen in LTO anodes.

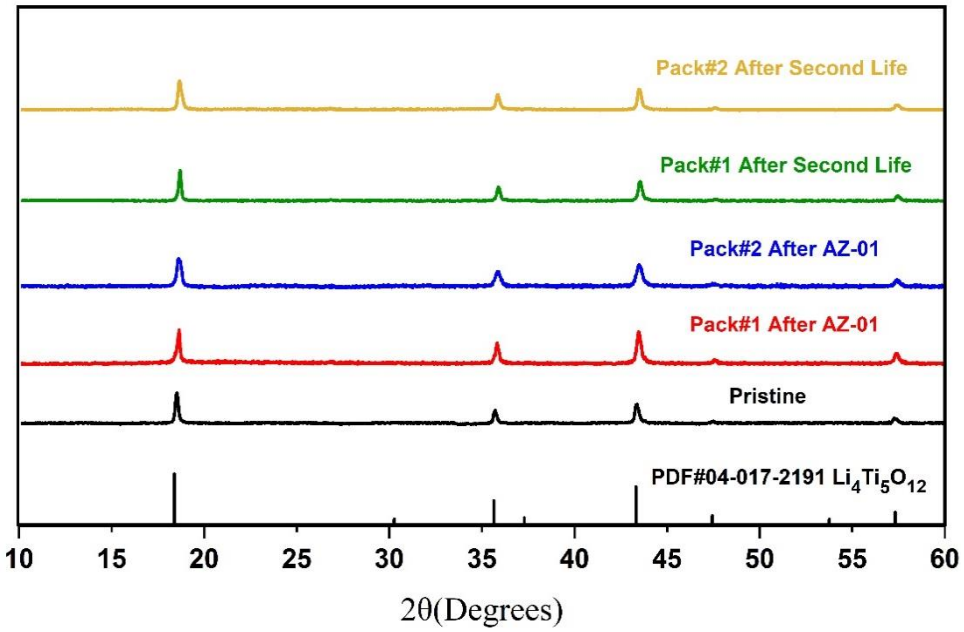

Figure 19: XRD patterns of LTO

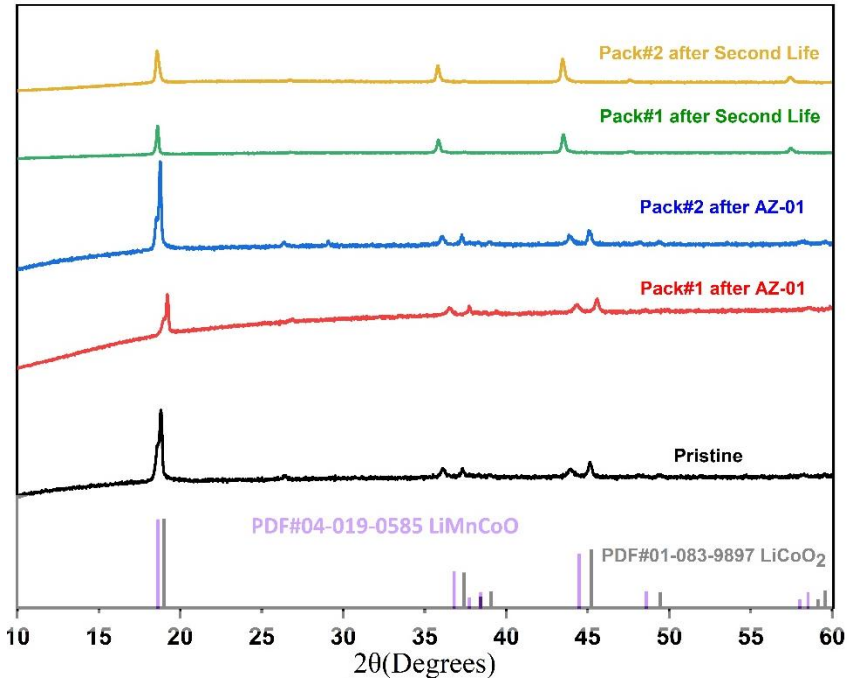

Figure 20: XRD patterns of LCO

Table 3: Rietveld Analysis of LCO Anode

SAMPLE	CELL VOLUME (Å^3)	A(Å)	STRAIN
PRISTINE LTO	584.06741	8.359	0.0001
PACK#1, AFTER AZ-01	584.06741	8.359	0.00010062
PACK#2, AFTER AZ-01	584.06741	8.359	0.00013966
PACK#1, AFTER SL	584.06741	8.3592	0.09580225
PACK#2, AFTER SL	583.63322	8.35692	0.00016
FAULTED PACK#2	622.61709	8.539	2.004535

The LTO anode shows excellent structural stability against ageing and no major changes in the peak are observed. Lattice parameters and strains calculated from Rietveld from the refinement are tabulated in Table 1 and Table 2 for LTO and LCO respectively.

Table 4: Rietveld Analysis of LCO cathode

Sample	Cell Volume ($Å^3$)	a(Å)	c(Å)	Strain
Pristine LCO	98.69127	2.822097	14.30972	0.622
Pack#1, After AZ-01	104.86312	2.921616	14.1855	0.13
Pack#2, After AZ-01	102.69431	2.863103	14.46577	2.03413
Pack#1, After SL	98.03898	2.814809	14.28796	0.659162
Pack#2, After SL	98.499	2.807	14.435	0.23098

The LTO anodes show little or no strain even after Second-Life cycling, the lattice strains were not observed. One cell from Pack#2 was observed to be swollen and failed, but no flames were seen, and the process seems to be self-passivating as it does not propagate or affect the adjacent cells. Rietveld refinement reveals a highly distorted lattice for the faulted, swollen cell. Appendix C shows the results of phase identification of anode and cathode patterns as obtained using Jade software.

5 SHORTCOMINGS

It is noteworthy that battery packs under study were modules of 6 cells in parallel without an active balancing and failure in a single cell can affect the performance of the pack and would be hard to probe with current experimental setup. This is a major shortcoming of the experimental procedure adopted. Thus, resolving the Nyquist plot was difficult and non-conclusive, quantitively. An active control switch is necessary to be designed and implemented that will include complex electronic parts so that health of each cell can be monitored, this could be done using multiplexers that can probe individual cells as they get charged at a charging station. High precision voltage source (+/- 0.5mV) are essential to effectively resolve the voltage curves and quantitatively know the coulombic efficiency, the Arbin cyclers used has little accuracy as they were not calibrated in

due time had errors.

Sophisticated characterization techniques such as TEM and In-Situ X-ray that can probe changes in operation will provide better insight into the phenomenon behind cell behaviors and operation. To better probe the surface and features like SEI, advanced characterization (such as TEM/SEM) is crucial and will be done to observe dendrite growth at high rates and effects of temperature on active material surface. Also, the connections and soldering done to make the battery packs were not identical and may have caused noise in impedance spectra. Single cells and half cells that are identical should be tested for more accurate data on failure mechanism

6 CONCLUSIONS AND FUTURE WORK

The anode material was confirmed to be purely LTO however the cathode was found to be a mixture of LMO and LCO. A rise or fall of about 1.5 mAh was evident by cycling at 40°C. The first stage of gradual capacity fade is marked by the slow degradation of cathode. As the cell ages, cathode capacity fades faster and when its value reduces than that of anode, a second stage of capacity fade is observed which corresponds to the dwindling cathode capacity. Expectedly, XRD patterns of LTO shows no major change in the crystal structure, however, the XRD of LCO reveals that the cathode material is a mix of LCO and LMCO unlike stated by the manufacturer, which proves that the cathode material disintegrates which can be classified as Loss Of Active Material (LAM)This shows a different nature of Li^+ ion transport which occurs through a phase change (flat voltage curve while discharge with slopes at voltage boundaries) in the anode while. Li^+ transport

through cathode occurs via a solid solution route (steady voltage increases while charging). As the battery is cycled the loss of Manganese ions is seen, which is commonly observed mechanism of cathode ageing. A steady increase in the High Frequency Resistance (mainly R_1) and the trend of impedance spectra signifies Conduction Losses (CL) as the electrolyte partly reacts with cathode.

To test battery, it is essential to either have very accurate current supply and measure the decreasing coulombic efficiency or to test the batteries in a simulated environment and operating condition and observe capacity fade, however filtered Differential Voltage curve that is flat with two peaks for discharge prove that that there is a two-phase change in the LTO (anode) as Li^+ ions get transferred to the cathode during discharging The DVA curves are a tool to resolve degradation of individual failure mechanism by its features even when cells are probed in a parallel connection battery pack.

Loss of Active Material (LAM) can be concluded as the major degradation mechanism as evident from XRD and DVA curves that triggers other failure mechanism like CL and LLI to occur. RUL could not be estimated quantitively as it is important that single cells are tested along with battery packs to understand the electrochemistry of a cell and dynamics of cell working together in a pack. Efforts on finding the inflexion point between first stage of slow degradation and second stage of accelerated fading were made to decide the usability of a battery pack from vehicle ESS for use in stationary applications like grid storage (Second-Life).

Cell testing as presented in this thesis will be continued with efforts to actively and passively augment Supercapacitors along with LIBs to form a hybrid ESS. Extensive EIS and

cyclic voltammetry on lab assembled coin-cells (from sample cell's electrodes) can be used to resolve the behavior of each electrode and testing can be standardized for regulating data presented by battery manufacturers. A new approach towards testing should include the effects of electrolyte mixtures and additives on cell performance and characterization of electrolyte, a component that was overlooked in this testing, shall be emphasized. A robust testing procedure should include cycling of both, single cells and battery packs by using high precision cyclers to resolve the degradation of individual components of a cell along with characterization of cell in operation and post-mortem. Quantitative analysis can then be done to predict accurately Remaining Useful Life of a cell or a battery pack.

7 REFERENCES

[1] Warner, J. T. (2015). The handbook of lithium-ion battery pack design: chemistry, components, types and terminology. Elsevier.

[2] Daniell, J. F. (1836). X. On Voltaic Combinations. In a letter addressed to Michael Faraday, DCL, FRS, Fullerian Prof. Chem. Royal Institution, Corr. Memb. Royal & Imp. Acadd. of Science, Paris, Petersburgh, &c. By J. Frederic Daniell, FRS, Prof. Chem. in King's College, London. Philosophical Transactions of the Royal Society of London, (126), 107-124.

[3] Jayson, J. S. (2014). The Daniell cell, Ohm's law, and the emergence of the International System of Units. American Journal of Physics, 82(1), 60-65.

[4] Kurzweil, P. (2010). Gaston Planté and his invention of the lead–acid battery—The genesis of the first practical rechargeable battery. Journal of Power Sources, 195(14), 4424-4434.

[5] Williams, J. B. (2018). Portable Power: Batteries. In The Electric Century (pp. 84-92). Springer, Cham.

[6] Sarma, D. D., & Shukla, A. K. (2018). Building Better Batteries: A Travel Back in Time.

[7] Whittingham, M. S. (1977). U.S. Patent No. 4,009,052. Washington, DC: U.S. Patent and Trademark Office.

[8] Padhi, A. K., Nanjundaswamy, K. S., & Goodenough, J. B. (1997). Phospho-olivines as positive-electrode materials for rechargeable lithium batteries. Journal of the electrochemical society, 144(4), 1188-1194.

[9] Ozawa, K. (1994). Lithium-ion rechargeable batteries with LiCoO2 and carbon electrodes: the LiCoO2/C system. Solid State Ionics, 69(3-4), 212-221.

[10] Croce, F., Appetecchi, G. B., Persi, L., & Scrosati, B. (1998). Nanocomposite polymer electrolytes for lithium batteries. Nature, 394(6692), 456.

[11] Curry, C. (2017). Lithium-ion battery costs and market. Bloomberg New Energy Finance, 5.

[12] Johnson, B. A., & White, R. E. (1998). Characterization of commercially available lithium-ion batteries. Journal of power sources, 70(1), 48-54.

[13] Pfenninger, R., Afyon, S., Garbayo, I., Struzik, M., & Rupp, J. L. (2018). Lithium Titanate Anode Thin Films for Li-Ion Solid State Battery Based on Garnets. Advanced Functional Materials, 28(21), 1800879.

[14] Patoux, S., Sannier, L., Lignier, H., Reynier, Y., Bourbon, C., Jouanneau, S., ... & Martinet, S. (2008). High voltage nickel manganese spinel oxides for Li-ion batteries. Electrochimica Acta, 53(12), 4137-414

[15] Ding, Y., Cano, Z. P., Yu, A., Lu, J., & Chen, Z. (2019). Automotive Li-Ion Batteries: Current Status and Future Perspectives. Electrochemical Energy Reviews, 1-28.

[16] Global EV Outlook 2018: Key Findings. (n.d.). Retrieved from https://www.iea.org/gevo2018/

[17] Thackeray, M. M., Wolverton, C., & Isaacs, E. D. (2012). Electrical energy storage for transportation—approaching the limits of, and going beyond, lithium-ion batteries. *Energy & Environmental Science*, *5*(7), 7854. doi:10.1039/c2ee21892e

[18] Goodenough, J. B., & Kim, Y. (2010). Challenges for Rechargeable Li Batteries†. *Chemistry of Materials*, *22*(3), 587-603. doi:10.1021/cm901452z

[19] Debnath, U. K., Ahmad, I., & Habibi, D. (2014). Quantifying economic benefits of second life batteries of gridable vehicles in the smart grid. International Journal of Electrical Power & Energy Systems, 63, 577-587.

[20] Lin, D., Liu, Y., Liang, Z., Lee, H. W., Sun, J., Wang, H., & Cui, Y. (2016). Layered reduced graphene oxide with nanoscale interlayer gaps as a stable host for lithium metal anodes. Nature nanotechnology, 11(7), 626.

[21] He, Y. B., Liu, M., Huang, Z. D., Zhang, B., Yu, Y., Li, B., ... & Kim, J. K. (2013). Effect of solid electrolyte interface (SEI) film on cyclic performance of Li4Ti5O12 anodes for Li ion batteries. Journal of Power Sources, 239, 269-276.

[22] Takami, N., Inagaki, H., Kishi, T., Harada, Y., Fujita, Y., & Hoshina, K. (2009). Electrochemical Kinetics and Safety of 2-Volt Class Li-Ion Battery System Using Lithium Titanium Oxide Anode. Journal of The Electrochemical Society, 156(2), A128. doi:10.1149/1.3043441

[23] Zaghib, K., Dontigny, M., Guerfi, A., Charest, P., Rodrigues, I., Mauger, A., & Julien, C. (2011). Safe and fast-charging Li-ion battery with long shelf life for power applications. Journal of Power Sources, 196(8), 3949-3954. doi:10.1016/j.jpowsour.2010.11.093

[24] He, Y., Liu, M., Huang, Z., Zhang, B., Yu, Y., Li, B., … Kim, J. (2013). Effect of solid electrolyte interface (SEI) film on cyclic performance of Li4Ti5O12 anodes for Li ion batteries. Journal of Power Sources, 239, 269-276.doi:10.1016/j.jpowsour.2013.03.141

[25] Colbow, K. M., Dahn, J. R., & Haering, R. R. (1989). Structure and electrochemistry of the spinel oxides LiTi2O4 and Li43Ti53O4. Journal of Power Sources, 26(3-4), 397-402.

[26] Sun, X., Radovanovic, P. V., & Cui, B. (2015). Advances in spinel Li 4 Ti 5 O 12 anode materials for lithium-ion batteries. New Journal of Chemistry, 39(1), 38-63.

[27] Kim, S. H., Choi, K. H., Cho, S. J., Yoo, J., Lee, S. S., & Lee, S. Y. (2018). Flexible/shape-versatile, bipolar all-solid-state lithium-ion batteries prepared by multistage printing. Energy & Environmental Science,11(2), 321-330.

[28]Yun, B. N., Du, H. L., Hwang, J. Y., Jung, H. G., & Sun, Y. K. (2017). Improved electrochemical performance of boron-doped carbon-coated lithium titanate as an anode material for sodium-ion batteries. Journal of Materials Chemistry A, 5(6), 2802-2810.

[29] Amine, K., Belharouak, I., Chen, Z., Tran, T., Yumoto, H., Ota, N., ... & Sun, Y. K. (2010). Nanostructured anode material for high-power battery system in electric vehicles. Advanced materials, 22(28), 3052-3057.

[30] Vilppo, O., & Markkula, J. (2015). Feasibility of electric buses in public transport. World Electric Vehicle Journal, 7(3), 357-365.

[31] Horiba, T. (2014). Lithium-ion battery systems. Proceedings of the IEEE, 102(6), 939-950.

[32] Feng, X., Li, J., Ouyang, M., Lu, L., Li, J., & He, X. (2013). Using probability density function to evaluate the state of health of lithium-ion batteries. Journal of Power Sources, 232, 209-218.

[33] Tong, S. J., Same, A., Kootstra, M. A., & Park, J. W. (2013). Off-grid photovoltaic vehicle charge using second life lithium batteries: An experimental and numerical investigation. Applied energy, 104, 740-750.

[34] Wang, Y., Chu, Z., Feng, X., Han, X., Lu, L., Li, J., & Ouyang, M. (2018). Overcharge durability of Li4Ti5O12 based lithium-ion batteries at low temperature. Journal of Energy Storage, 19, 302-310.

[35] Liu, S., Winter, M., Lewerenz, M., Becker, J., Sauer, D. U., Ma, Z., & Jiang, J. (2019). Analysis of cyclic aging performance of commercial Li4Ti5O12-based batteries at room temperature.

[36] Han, X., Ouyang, M., Lu, L., Li, J., Zheng, Y., & Li, Z. (2014). A comparative study of commercial lithium ion battery cycle life in electrical vehicle: Aging mechanism identification. Journal of Power Sources, 251, 38-54. doi: 10.1016/j.jpowsour.2013.11.029

[37] Han, X., Ouyang, M., Lu, L., & Li, J. (2014). Cycle life of commercial lithium-ion batteries with lithium titanium oxide anodes in electric vehicles. Energies, 7(8), 4895-4909.

[38] Xiong, R., Gong, X., Mi, C. C., & Sun, F. (2013). A robust state-of-charge estimator for multiple types of lithium-ion batteries using adaptive extended Kalman filter. Journal of Power Sources, 243, 805-816.

[39] Peterson, S. B., Apt, J., & Whitacre, J. (2010). Lithium-ion battery cell degradation resulting from realistic vehicle and vehicle-to-grid utilization. Journal of Power Sources, 195(8), 2385-2392. doi: 10.1016/j.jpowsour.2009.10.010

[40] Xie, H., Zheng, S., & Ni, M. (2017). Microgrid Development in China: A method for renewable energy and energy storage capacity configuration in a megawatt-level isolated microgrid. IEEE Electrification Magazine, 5(2), 28-35.

[41] Dai, H., Jiang, B., & Wei, X. (2018). Impedance characterization and modeling of lithium-ion batteries considering the internal temperature gradient. Energies, 11(1), 220.

[42] Xu, J., Mi, C. C., Cao, B., & Cao, J. (2013). A new method to estimate the state of charge of lithium-ion batteries based on the battery impedance model. Journal of power sources, 233, 277-284.

[43] Jow, T. R., Delp, S. A., Allen, J. L., Jones, J. P., & Smart, M. C. (2018). Factors limiting Li+ charge transfer kinetics in Li-ion batteries. Journal of The Electrochemical Society, 165(2), A361-A367

[44] Pastor-Fernández, C., Uddin, K., Chouchelamane, G. H., Widanage, W. D., & Marco, J. (2017). A comparison between electrochemical impedance spectroscopy and incremental capacity-differential voltage as Li-ion diagnostic techniques to identify and quantify the effects of degradation modes within battery management systems. Journal of Power Sources, 360, 301-318.

[45] Dubarry, M., Svoboda, V., Hwu, R., & Yann Liaw, B. (2006). Incremental Capacity Analysis and Close-to-Equilibrium OCV Measurements to Quantify Capacity Fade in Commercial Rechargeable Lithium Batteries. Electrochemical and Solid-State Letters, 9(10), A454. doi:10.1149/1.2221767

[46] Hall, F., Touzri, J., Wußler, S., Buqa, H., & Bessler, W. G. (2018). Experimental investigation of the thermal and cycling behavior of a lithium titanate-based lithium-ion pouch cell. Journal of Energy Storage, 17, 109-117.

[47] Deschanvres, A., Raveau, B., & Sekkal, Z. (1971). Mise en evidence et etude cristallographique d'une nouvelle solution solide de type spinelle Li1+ xTi2− xO4 0⩽ x⩽ 0, 333. Materials Research Bulletin, 6(8), 699-704.

[48] Kataoka, K., & Akimoto, J. (2014). Single-crystal growth, crystal structure analysis and physical properties of lithium over stoichiometric Li1+ xCoO2. Solid State Ionics, 262, 106-109.

[49] Kim, K. M., Kim, S., Lee, Y. G., & Kim, J. Electrochemical Properties of Mixed Cathode Consisting of μm-Scale LiCoO2 and nm-Scale.

[50] Wohlfahrt-Mehrens, M., Vogler, C., & Garche, J. (2004). Aging mechanisms of lithium cathode materials. Journal of power sources, 127(1-2), 58-64.

APPENDIX A

SCHEDULE FOR BATTERY CYCLING

		Step Label	Number Of Limits	Control Type	Control Value	Extra Control Value 1	Extra Control Value 2	Current Range	Extended Definition	Extended Definition 1		Log Clock Stretch	
1		Rest	1	Rest									
		Log Limit	Step Limit	Goto Step	Variable1	Operator1	Value1	Variable2	Operator2	Value2	Variable3	Operator3	Value3
	1	✓	✓	Next Step	PV_CHAN_Step_Time	>=	00:02:00						
2		Charge	2	Current(A)	7.8			High					
		Log Limit	Step Limit	Goto Step	Variable1	Operator1	Value1	Variable2	Operator2	Value2	Variable3	Operator3	Value3
	1	✓	✓	Next Step	PV_CHAN_Voltage	>=	2.85						
	2	✓			DV_Time	>=	00:00:10						
3		Rest 2	1	Rest									
4		Cycling	3	Current Simulation	AZ01.txt			High					
		Log Limit	Step Limit	Goto Step	Variable1	Operator1	Value1	Variable2	Operator2	Value2	Variable3	Operator3	Value3
	1	✓	✓	LOOP	PV_CHAN_Step_Time	>=	00:44:27						
	2	✓	✓	Charge2	PV_CHAN_Voltage	<=	1.5						
	3	✓			DV_Time	>=	00:00:01						
5		LOOP	1	Set Variable(s)	Reset	Increment	Decrement						
		Log Limit	Step Limit	Goto Step	Variable1	Operator1	Value1	Variable2	Operator2	Value2	Variable3	Operator3	Value3
	1	✓	✓	Cycling	PV_CHAN_Cycle_Index	<=	1000						
6		Charge2	2	Current(A)	7.8			High					
		Log Limit	Step Limit	Goto Step	Variable1	Operator1	Value1	Variable2	Operator2	Value2	Variable3	Operator3	Value3
	1	✓	✓	Next Step	PV_CHAN_Voltage	>=	2.85						
	2	✓			DV_Time	>=	00:00:10						
7		Rest 3	1	Rest									
8		Cycling2	3	Current Simulation	AZ01.txt			High					
9		LOOP2	1	Set Variable(s)	Reset	Increment	Decrement						
10		Charge 3	2	Current(A)	7.8			High					
11		Rest4	1	Rest									
12		Cycling 3	3	Current Simulation	AZ01.txt			High					
13		LOOP3	1	Set Variable(s)	Reset	Increment	Decrement						
14		Charge 4	2	Current(A)	7.8			High					
15		Rest 5	1	Rest									
16		Cycling 4	3	Current Simulation	AZ01.txt			High					
17		LOOP4	1	Set Variable(s)	Reset	Increment	Decrement						
18		Charge 5	2	Current(A)	7.8			High					
19		Rest 6	1	Rest									
20		Cycling 5	3	Current Simulation	AZ01.txt			High					
21		LOOP5	1	Set Variable(s)	Reset	Increment	Decrement						
22		Charge 6	2	Current(A)	7.8			High					
23		Rest 7	1	Rest									
24		Cycling 6	3	Current Simulation	AZ01.txt			High					
		Log Limit	Step Limit	Goto Step	Variable1	Operator1	Value1	Variable2	Operator2	Value2	Variable3	Operator3	Value3
	1	✓	✓	LOOP6	PV_CHAN_Step_Time	>=	00:44:27						
	2	✓	✓	Rest End	PV_CHAN_Voltage	<=	1.5						
	3	✓			DV_Time	>=	00:00:01						
25		LOOP6	1	Set Variable(s)	Reset	Increment	Decrement						
		Log Limit	Step Limit	Goto Step	Variable1	Operator1	Value1	Variable2	Operator2	Value2	Variable3	Operator3	Value3
	1	✓	✓	Cycling 6	PV_CHAN_Cycle_Index	<=	1000						
26		Rest End	1	Rest									
		Log Limit	Step Limit	Goto Step	Variable1	Operator1	Value1	Variable2	Operator2	Value2	Variable3	Operator3	Value3
	1	✓	✓	Next Step	PV_CHAN_Step_Time	>=	00:05:00						
27		Constant Charge	2	Current(A)	1.56			Medium					
		Log Limit	Step Limit	Goto Step	Variable1	Operator1	Value1	Variable2	Operator2	Value2	Variable3	Operator3	Value3
	1	✓	✓	Next Step	PV_CHAN_Voltage	>=	2.85						
	2	✓			DV_Time	>=	00:00:10						
28		Rest Final	1	Rest									
29		Constant Discharg	2	Current(A)	-1.56			Medium					
		Log Limit	Step Limit	Goto Step	Variable1	Operator1	Value1	Variable2	Operator2	Value2	Variable3	Operator3	Value3
	1	✓	✓	Next Step	PV_CHAN_Voltage	<=	1.5						
	2	✓			DV_Time	>=	00:00:10						
30		LOOP FINAL	2	Set Variable(s)	Reset	Increment	Decrement						
		Log Limit	Step Limit	Goto Step	Variable1	Operator1	Value1	Variable2	Operator2	Value2	Variable3	Operator3	Value3
	1	✓	✓	End Test	TC_Counter1	>	5						
	2		✓	Charge	TC_Counter1	<=	5						

APPENDIX B

CAPACITY FADE AND DIFFERENTIAL VOLTAGE

Two stage capacity fade observed in cells with LTO anode and NCM cathode [37]

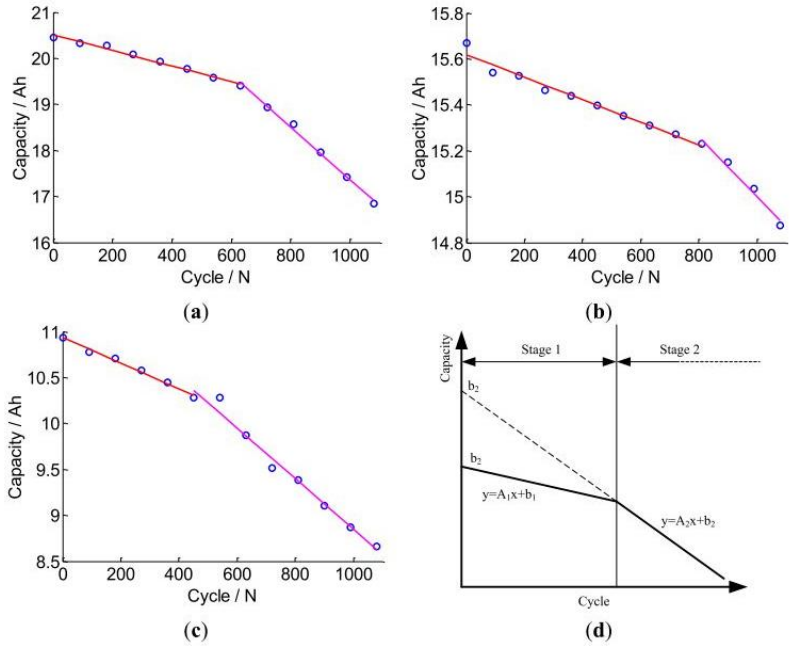

Differential Voltage curves of LTO battery [37]

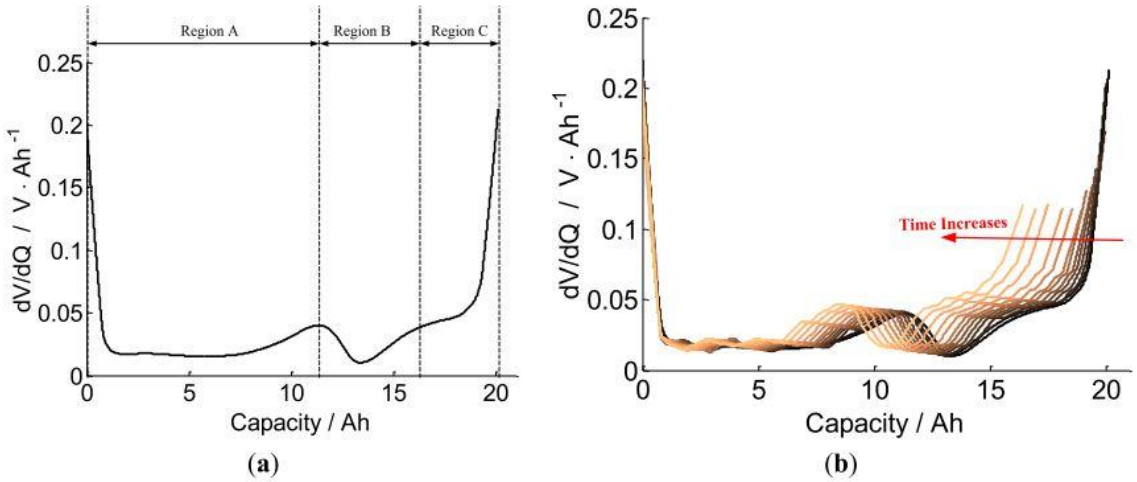

APPENDIX C

XRD PHASE RECOGNITION USING JADE FOR ELECTRODES

XRD phase recognition for anode using Jade

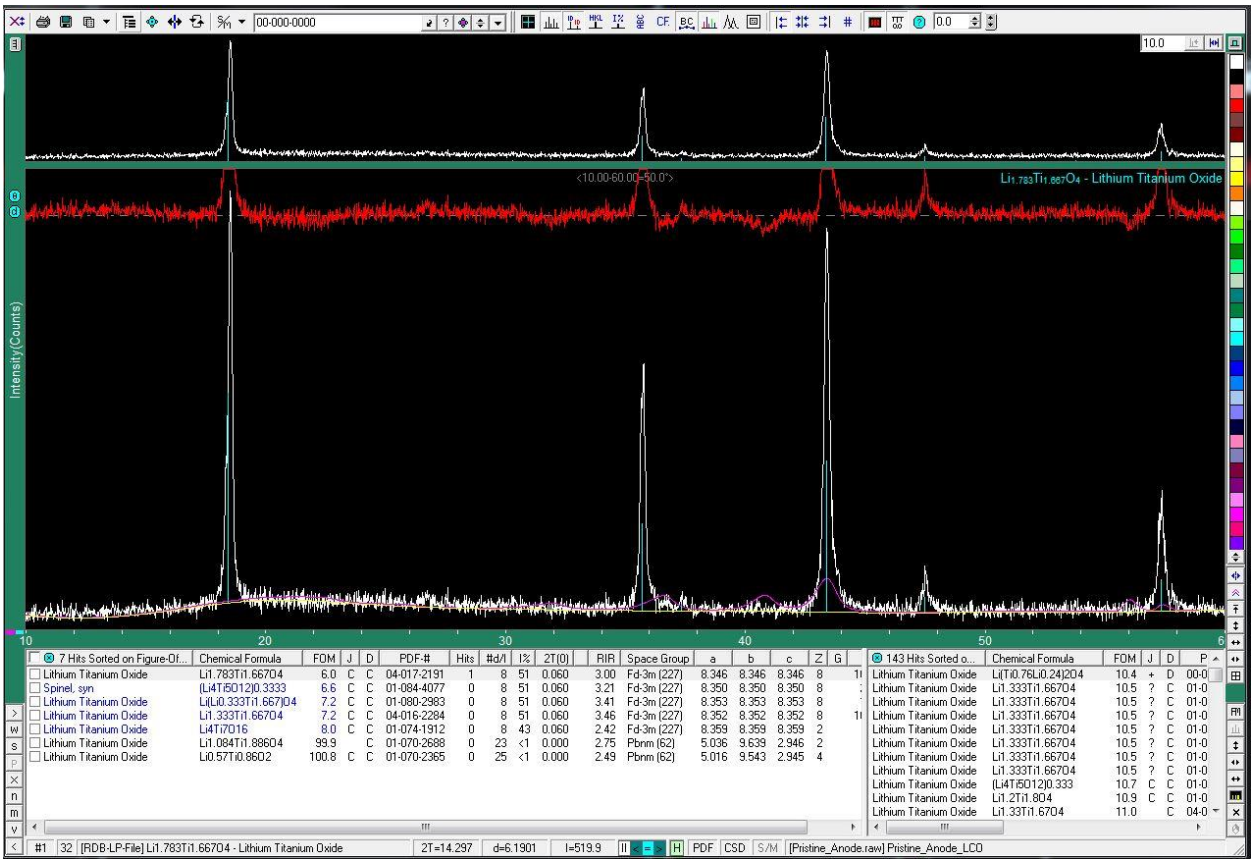

XRD phase recognition for cathode using Jade